Nonreciprocal Remanence Phase Shifters in Rectangular Waveguide

WILLIAM J. INCE AND ERNEST STERN

Abstract—**Three types of nonreciprocal remanent phase shifters in rectangular waveguide are described which are approximated by a simple model consisting of twin ferrite slabs symmetrically placed in rectangular waveguide and separated by a dielectric rib. The model has been analyzed with the assumption that a fundamental TE mode wave propagates in the structure. Simultaneous solution of Maxwell's equations in the three regions of dielectric, ferrite, and air within the waveguide enables the characteristic equation to be formed. The characteristics of the model have been obtained with the aid of a computer as a function of dimensions, dielectric and magnetic constants, frequency, and power. The theoretical results are compared with experimental data obtained on a double toroid structure. Correction factors applied to the experimental data, which are necessary to account for differences between the practical structure and the ideal model, are discussed.**

Introduction

CONSIDERABLE attention is being given to the development of ferrite phase shifters, capable of handling peak power in the range 10^4 to 10^5 watts and requiring the minimum of control power, for use as beam-steering elements in phased-array radars [1]. The concept of using ferrite microwave phase shifters for inertialless scanning of radar beams is not new. However, the need for a phaser which can be switched in a few microseconds has caused the recent emphasis in phase shifter development to be placed on the latching, or remanent, ferrite phaser. A square loop ferrite[1] is arranged in a closed magnetic path, the two remanent states of magnetization corresponding to the two stable states of the phase shifter. Hence, control power is only required when switching between states, as in the case of a computer memory core. The bistatic characteristics of the remanent phase shifter make it an attractive device for use in phased-array systems utilizing digital computer control.

Treuhaft and Silber [2] first recognized the advantage of using square loop microwave toroids in phase shifters as a means of eliminating the steady magnetizing current and reducing the switching energy required. Stern and Hair [3] applied this concept to a remanence phase shifter in helical transmission line. These phase shifters are of the nonreciprocal type, in which the magnetization is transverse to the direction of propagation. The toroidal phase shifter in rectangular waveguide can be approximated by the twin slab configuration, which has been analyzed by Lax and Button [5] and more recently by Ince and Stern [6], and by Schlomann [7]. In this paper, a more complete analysis is presented, which includes the effect of dielectric loading and considers the effects of small dielectric and magnetic losses on the performance. The configuration analyzed, shown in Fig. 1, is the foundation of several nonreciprocal remanent shifters. The model consists of two ferrite slabs symmetrically located in rectangular waveguide and separated by a dielectric rib. The slabs are magnetized in opposite directions, both transverse to the direction of propagation.

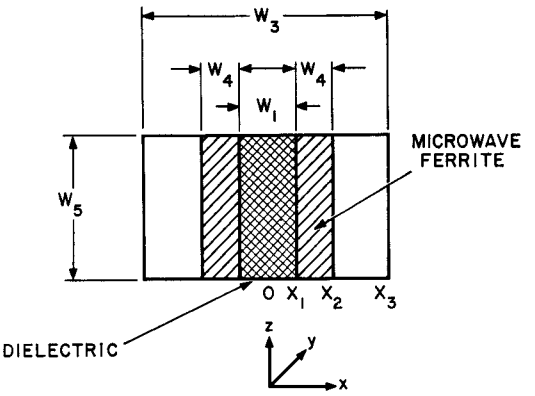

Fig. 1. Theoretical model of remanence phase shifter.

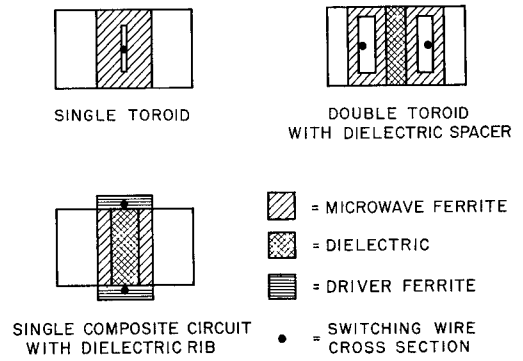

Fig. 2. Nonreciprocal remanence phase shifter configurations.

Three practical remanent phaser structures are illustrated in Fig. 2. The first diagram shows a single rectangular toroid located at the center of the waveguide [2]. In the double toroid phaser, the toroids are symmetrically placed in the waveguide and are separated by a dielectric rib. This configuration permits the use of large slots in the toroids that are easily machined or extruded, and eliminates coupling of microwave energy to the control wires. The composite cir-

Manuscript received April 20, 1966; revised September 28, 1966.

The authors are with the Lincoln Laboratory, Massachusetts Institute of Technology, Lexington, Mass. (Operated with support from the U. S. Advanced Research Projects Agency.)

[1] For a detailed discussion of the major factors determining squareness of hysteresis loops in ferrites, such as crystalline anisotropy, magnetostriction, shape, anisotropy, and porosity, see Wijn et al. [4].

cuit phaser [8], [9] is useful in applications where temperature stability is important. Part of the magnetic circuit is formed by a ferrite which has a high Curie temperature and which limits the flux in the circuit. In the figure, the flux path is completed external to the microwave circuit by the use of thin-walled waveguides.

Characterization of Remanent Ferrite

The tensor permeability of the remanent ferrite for the lossless case is taken to be of the form

$$\frac{\mu\pm}{\mu_0} = \begin{bmatrix} 1 & \mp\frac{jm}{F} & 0 \\ \pm\frac{jm}{F} & 1 & 0 \\ 0 & 0 & 1 \end{bmatrix}. \tag{1}$$

The remanent magnetization, $4\pi M_r$, has been normalized with respect to the applied center frequency, ω_0, to form the dimensionless parameter m, equal to $\gamma 4\pi M_r/\omega_0$. The normalized frequency F is equal to ω/ω_0, where ω is the applied frequency. The magnetization is considered positive if the RF magnetic field rotates in a clockwise direction.

This form of the permeability tensor implies that the average internal magnetizing field is small, and that the number of domains in the remanent material which are at resonance, due to the magnitude of the internal field, is also small. Rado [10] has discussed the magnetic losses observed in various polycrystalline unmagnetized ferrites. At sufficiently high frequencies, where domain wall motion can be neglected, the losses of the remanent ferrite may be attributed to rotational resonance. According to the theory of Polder and Smit [11], the resonant frequency of an individual domain can extend up to a maximum frequency given by

$$\omega_{\max} = \gamma[H_{\text{anis}} + 4\pi M_s]$$

where H_{anis} is the effective anisotropy field and $4\pi M_s$ the saturation magnetization. Hence, it can be anticipated that the radio $\gamma 4\pi M_s/\omega$ must be less than unity in order to reduce the small signal magnetic loss. This general rule is found to apply for many microwave ferrites. Correspondingly, m is also restricted in value, as will be shown later.

By assuming appropriate demagnetizing factors, it can be shown that for phase shifter geometries in which the toroid length is much greater than its wall thickness, the toroid shape has little effect on the components of the permeability tensor when m is less than unity.

Derivation of the Characteristic Equation

We assume the steady-state transverse electric field of the fundamental mode to be parallel to the z-axis and given by $e = E(x)e^{j\beta y}$. An exponential time dependence is implied. The coordinate system used here permits us to conform with the practice of reserving the z-axis for the direction of the steady magnetization.

The electric field distribution across the waveguide is assumed to be

$$E_{z_1} = E_1 \cos(2\pi F K_1 x) \text{ volt/m}$$

$$E_{z_2} = E_2 \exp(j2\pi F K_2 x) + E_4 \exp(-j2\pi F K_2 x) \text{ volt/m}$$

$$E_{z_3} = E_3 \sin[2\pi F K_3(x_3 - x)] \text{ volt/m}$$

where E_1, E_2, E_3, E_4 are complex numbers. If any of the corresponding eigenvalues K_1, K_2, or K_3 are imaginary, E_{z_1} and E_{z_3} become hyperbolic functions. The suffixes, 1, 2, 3, refer to the dielectric, ferrite, or air regions, respectively, within the waveguide. The dimensions of the model are expressed in normalized form, enabling the analysis to be performed in a general manner, so that the results are applicable to the entire microwave spectrum.

Substitutions of the above trial solutions into Maxwell's equations yield the equations for the magnetic field distribution:

$$H_{x_1} = \eta E_1 p \cos(2\pi F K_1 x) \text{ amps/m} \tag{1a}$$

$$H_{y_1} = j\eta E_1 K_1 \sin(2\pi F K_1 x) \text{ amps/m} \tag{1b}$$

$$H_{x_2} = \frac{2\eta E}{(1-m^2)}\{p[r\cos(2\pi F K_2 x) - \sin(2\pi F K_2 x)] \pm mK_2[r\sin(2\pi F K_2 x) + \cos(2\pi F K_2 x)]\} \text{ amps/m} \tag{1c}$$

$$H_{y_2} = \frac{j2\eta E}{(1-m^2)}\{\pm mp[r\cos(2\pi F K_2 x) - \sin(2\pi F K_2 x)] + K_2[r\sin(2\pi F K_2 x) + \cos(2\pi F K_2 x)]\} \text{ amps/m} \tag{1d}$$

$$H_{x_3} = \eta p E_3 \sin(2\pi F K_3(x_3 - x)) \text{ amps/m} \tag{1e}$$

$$H_{y_3} = j\eta K_3 E_3 \cos[2\pi F K_3(x_3 - x)] \text{ amps/m} \tag{1f}$$

where p is the ratio of free space to guide wavelength, λ/λ_g.

$$\left(\frac{2\pi}{\lambda}\right)p = \beta$$

$$\eta = \sqrt{\frac{\epsilon_0}{\mu_0}}$$

and

$$E_2 = E_4{}^* = E(r + j). \tag{2}$$

Introduction of the parameters E and r enable more compact expressions for the Poynting vector and dissipation to be obtained. The alternate forms of the magnetic field equations, for imaginary eigenvalues, are obtained by substituting jK_i for K_i.

In order for the solution of Maxwell's equations to be self-consistent, a set of three simultaneous equations involving p must be satisfied:

$$K_1{}^2 = \epsilon_1' - p^2 \tag{3}$$

$$K_2{}^2 = \epsilon_2'(1 - m^2) - p^2 \tag{4}$$

$$K_3{}^2 = \epsilon_3' - p^2 \tag{5}$$

where

$$\epsilon_1' = \frac{\epsilon_1}{\epsilon_0}, \text{ etc.}$$

The boundary conditions require that the tangential electric fields on the two sides of each interface are equal.

At the region 1–2 interface,

$$E_1 \cos \theta_1 = E_2 e^{j\theta_2} + E_4 e^{-j\theta_2}. \tag{6}$$

At the region 2–3 interface,

$$E_3 \sin \theta_3 = E_2 e^{j\theta_4} + E_4 e^{-j\theta_4}. \tag{7}$$

The simultaneous solution of (3), (4), and (5) with the aid of (6) and (7) yields the eigenfunction or characteristic equation.

$$\frac{\tan (\theta_4 - \theta_2)}{K_2} = \frac{K_3 \cot \theta_3 - K_1 \tan \theta_1}{(\epsilon_2' - p^2) + (1 - m^2)K_1K_3 \tan \theta_1 \cot \theta_3 \pm mp(K_3 \cot \theta_3 + K_1 \tan \theta_1)}. \tag{8}$$

Also,

$$r = \frac{K_2 + [(1 - m^2)K_3 \cot \theta_3 \mp mp] \tan \theta_4}{[(1 - m^2)K_3 \cot \theta_3 \mp mp] - K_2 \tan \theta_4} \tag{9}$$

where

$$\theta_1 = 2\pi F K_1 x_1$$

$$(\theta_4 - \theta_2) = 2\pi F K_2 (x_2 - x_1)$$

$$\theta_3 = 2\pi F K_3 (x_3 - x_2)$$

$$\theta_4 = 2\pi F K_2 x_2.$$

For real K_2, E is the amplitude of the imaginary part of E_2, and r is the ratio of the real and imaginary parts.

Power Flow

The Poynting vector, S, corresponds to power flow in the y-direction, which is given by

$$P = \int_{-x_3}^{+x_3} \int_0^{z_1} S(x)dx\,dz$$

$$= 2\lambda_0^2 z_1 \left\{ \frac{1}{2} \int_0^{x_1} E_{z1} H_{x1}^* dx + \frac{1}{2} \int_{x_1}^{x_2} E_{z2} H_{x2}^* dx + \frac{1}{2} \int_{x_2}^{x_3} E_{z3} H_{x3}^* dx \right\} \text{ watts.} \tag{10}$$

It is possible to write the power flow for each region as a function of the parameter $|E|^2$, defined by (2), by use of the boundary equations (6) and (7). Hence,

$$\frac{|E_1|^2}{|E|^2} = \left| \frac{4C_{22}}{1 + \cos 2\theta_1} \right| \quad \text{and} \quad \frac{|E_3|^2}{|E|^2} = \left| \frac{4C_{24}}{1 - \cos 2\theta_3} \right|.$$

Insertion of the appropriate field expressions into (10) enables the integration to be carried out. For region 1

$$P_1 = \eta F z_1 \lambda^2 |E|^2 \frac{C_1 C_{22}}{K_1}.$$

For region 2

$$P_2 = \eta F z_1 \lambda^2 |E|^2 \left[\frac{(C_{44} - C_{42})}{K_2} \mp \frac{m}{p} (C_{54} - C_{52}) \right].$$

For region 3

$$P_3 = \eta F z_1 \lambda^2 |E|^2 \frac{C_3 C_{24}}{K_3}$$

where

$$C_1 = \left| \frac{\sin 2\theta_1 + 2\theta_1}{1 + \cos 2\theta_1} \right|$$

$$C_3 = \left| \frac{2\theta_3 - \sin 2\theta_3}{1 - \cos 2\theta_3} \right|$$

$$C_{2i} = (r^2 + 1) + (r^2 - 1) \cos 2\theta_i - 2r \sin 2\theta_i$$

$$C_{4i} = (r^2 + 1)2\theta_i + (r^2 - 1) \sin 2\theta_i + 2r \cos 2\theta_i$$

$$C_{5i} = 2r \sin 2\theta_i - (r^2 - 1) \cos 2\theta_i \qquad i = 2, 4.$$

Thus the total power flow is given by

$$P = \frac{\eta}{2\pi} F z_1 p \lambda^2 C |E|^2 \text{ watts} \tag{11}$$

where

$$C = \frac{C_1 C_{22}}{K_1} + \frac{(C_{44} - C_{42})}{K_2} \mp \frac{m}{p} (C_{54} - C_{52}) + \frac{C_3 C_{24}}{K_3}.$$

Losses

With the assumption that the loss tangents are small, we proceed to calculate the phase shifter low-power loss by considering the field distributions of the fundamental mode to be identical to those in the lossless case. This is a reasonable assumption if the magnetic and dielectric loss tangents are small.

The total loss per unit length is equal to the sum of the dielectric, magnetic, and wall losses:

$$\frac{dP}{dy} = 2\omega\lambda_0^2 z_1 \left\{ \frac{\epsilon_i''}{2} \int_0^{x_i} \boldsymbol{E}_i \cdot \boldsymbol{E}_i^* dx + \frac{\tan \delta_m}{2} \int_{x_1}^{x_2} \boldsymbol{H}_2 \cdot \boldsymbol{B}_2^* dx \right\} + 2\lambda_0 R_s \int_{\text{walls}} \frac{|H_s|^2}{2} dx \qquad i = 1, 2. \tag{12}$$

H_s is the microwave magnetic field at the wall surface, R_s is the surface resistivity, $\boldsymbol{B}_2$ is the microwave flux density in the ferrite, and $\tan \delta_m$ is the magnetic loss tangent of the ferrite. The loss occurs, in part, in microscopic regions which are magnetized by fields ranging from zero to $(4\pi M_s + H_a)$. However, the average steady internal field is small; on the

order of the coercive force. With this assumption, the imaginary part of the off-diagonal component in the permeability tensor is taken to be negligible compared to the imaginary part of the diagonal component. Hence, the magnetic loss can be characterized in the bulk form by δ_m.

Solution of the previous integrals yields the following results.

Dielectric Losses:

$$\frac{z_1\lambda_0\eta}{2}|E|^2\left\{\frac{\epsilon_1''C_1C_{22}}{K_1}+\frac{\epsilon_2''(C_{44}-C_{42})}{K_2}+\frac{\epsilon_3''C_3C_{24}}{K_3}\right\}\text{watts/meter.}$$

Magnetic Losses:

$$\frac{z_1\lambda_0\eta}{2}|E|^2\left(\frac{\tan\delta_m}{K_2(1-m^2)}\right)[p^2(C_{44}-C_{42})+K_2^2(C_{74}-C_{72})\pm 2mpK_2(C_{54}-C_{52})]\text{ watts/meter.}$$

Wall Losses:

$$\frac{R_s\lambda_0\eta^2}{\pi F}|E|^2\left\{\frac{C_{22}}{K_1}K_1^2C_8+p^2C_1+\frac{C_{24}}{K_3}K_3^2(C_9+C_{10})+p^2C_3+\frac{(1+m^2)}{K_2(1-m^2)^2}p^2(C_{44}-C_{42})+K_2^2(C_{74}-C_{72})\pm\frac{4pK_2m}{1+m^2}(C_{54}-C_{52})\right\}$$

where

$$C_{7i}=(r^2+1)2\theta_i-(r^2-1)\sin 2\theta_i-2r\cos 2\theta_i \qquad i=2,4$$

$$C_8=\left|\frac{2\theta_1-\sin 2\theta_1}{1+\cos 2\theta_1}\right| \qquad C_9=\left|\frac{2\theta_3+\sin 2\theta_3}{1-\cos 2\theta_3}\right|$$

$$C_{10}=\frac{4\pi z_1FK_3}{|1-\cos 2\theta_3|} \qquad R_s=\sqrt{\frac{\pi f\mu_0}{\sigma}}.$$

The attenuation constant α is equal to $(1/P)(dP/dy)$ nepers, where P is given by (11).

Differential Phase Shift

Solutions of the characteristic equation, (8), for the rectangular waveguide case were obtained for specific combinations of parameter values by an iterative process, with the aid of the M.I.T. Lincoln Laboratory IBM 7094 computer. The ratio p, the free space to guide wavelength, has been plotted in Fig. 3 as a function of m. In this figure, the waveguide width corresponds to standard X-band waveguide at 10 GHz. There are two solutions, p^+ and p^-, corresponding to clockwise and counterclockwise orientation of the remanence flux about the direction of propagation in the twin-slab phase shifters of Fig. 2. The two curves intersect on the p-axis corresponding to pure dielectric loading and diverge at a fairly constant rate with increasing m. It follows that the differential phase shift per unit length, which is equal to $2\pi(p^- - p^+)/\lambda$, is an almost linear function of remanence magnetization. Quite large values of differential phase shift are obtained as m approaches unity. However, the greater the difference between p^- and p^+, the more difficult it becomes to maintain a match. Also, a value of m near unity is undesirable from loss considerations. Further computation has shown that the relationship between differential phase shift and m is linear to within a few percent for structures containing dielectrics with dielectric constants in the range 1 to 80, and for rib widths ranging from zero to 0.1 λ_0 in standard waveguide.

The variation of differential phase shift as a function of ferrite thickness is illustrated in Fig. 4, with the dielectric width W_1 as a parameter. The normalized remanence magnetization, m, is equal to 0.8. For some other value of m the differential phase shift is obtained by linearly scaling the curves of Fig. 4. The differential phase shift increases fairly linearly with ferrite thickness until there is sufficient volume of ferrite to support a large fraction of the total energy. Further increase in ferrite thickness merely adds material in a region where the energy density is low. If the ferrite near the center of the waveguide is replaced with a dielectric rib whose dielectric constant is comparable to that of the ferrite, the maximum phase shift remains the same. This suggests that the ferrite near the center of the waveguide contributes little to the differential phase shift. This is because the RF magnetic field is linearly polarized in the central region of the waveguide.

The magnetization at the corners of the toroid does not lie normal to the direction of the microwave field and, hence, is inefficient in producing differential phase shift. Consequently, this corner effect imposes a limit on the ferrite thickness.

Figure 4 indicates that the use of a dielectric rib can be extremely effective in boosting the differential phase shift. In Fig. 5 the differential phase shift obtained with a given pair of ferrite slabs has been plotted as a function of dielectric rib thickness. In this example, the ferrite thickness is 0.04 λ_0. Increasing the dielectric constant causes a very marked increase in the differential phase shift. Comparing the curves for ϵ_1' equal to 16 and 1 there is a ratio of at least 1.5 to 1 in differential phase shift. Note that the curves for high dielectric constants show pronounced maxima as a function of W_1. Beyond the maximum value the differential phase shift declines because the energy density in the ferrite is low. The value of ϵ_1' equal to 6 corresponds to the dielectric constant of beryllium oxide, which is a useful heat conductor for high-power applications, having low dielectric loss. The curve for this value of ϵ_1' exhibits considerably higher phase shift than for a simple air gap but, from phase shift considerations alone, one would probably use the highest possible dielectric constant.

One measure of the efficiency of a phase shifter is the ratio of the differential phase shift to the insertion phase of the device. We have found that this ratio is maximum if the ferrite width is between $0.04\lambda_0$ and $0.06\lambda_0$ for a wide range of dielectric rib parameters.

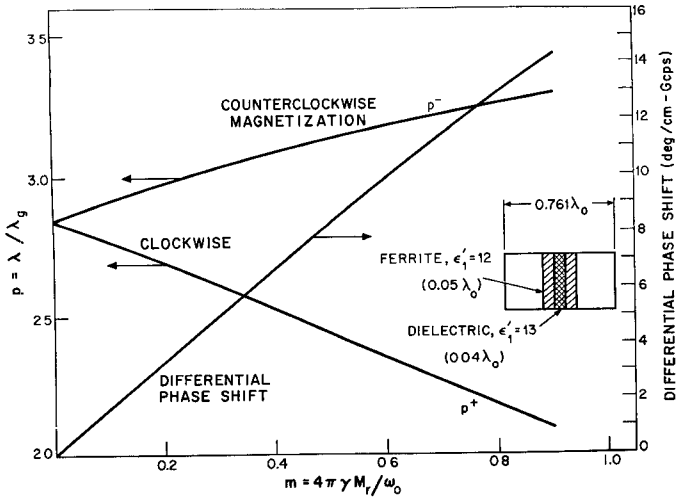

Fig. 3. Normalized waveguide wavelength and differential phase shift versus normalized remanence magnetization.

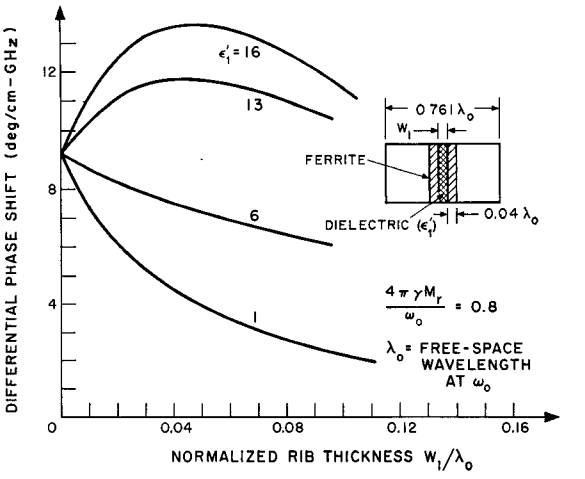

Fig. 5. Differential phase shift versus rib thickness for several dielectric constants.

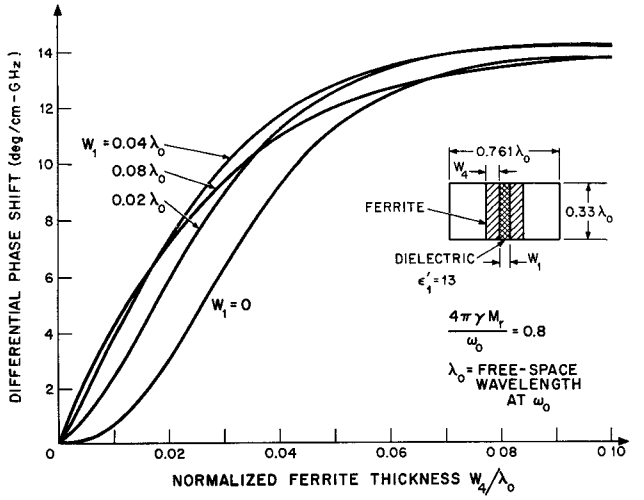

Fig. 4. Differential phase shift versus ferrite thickness for several dielectric thicknesses.

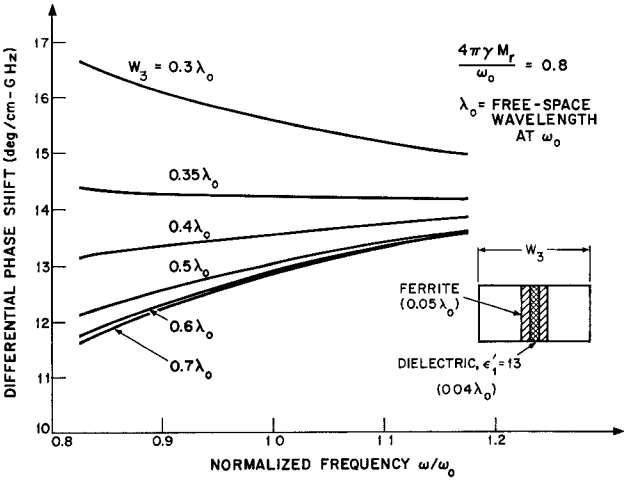

Fig. 6. Differential phase shift versus frequency for several waveguide widths.

Frequency Sensitivity

The differential phase versus frequency characteristic of the phase shifter can be controlled somewhat by appropriate choice of waveguide width. This is demonstrated in Fig. 6, in which the differential phase shift per unit length versus frequency for various waveguides, ranging from wide to quite narrow widths, are given. As the side walls are brought in, the curve changes from positive to negative slope. For the value $W_3 = 0.35\lambda_0$, the curve has zero slope, resulting in constant differential phase shift versus frequency. For very narrow waveguides, the p^+ mode approaches cut-off, presenting a matching problem as well as exhibiting higher attenuation. Nevertheless, the waveguide width can be reduced to about $0.3\lambda_0$ without serious deterioration of performance. In addition, since most of the energy is confined to the ferrite and dielectric regions, the use of narrow waveguide does not substantially degrade the peak power capacity of the device.

To some extent the frequency dependence of the differential phase shift can also be controlled by choice of the dielectric rib thickness, as can be seen in Fig. 11.

Magnetic Field Distribution

The complete RF magnetic field amplitude distributions [see (1)] were computed for the three regions within the phase shifter for a particular structure. The distributions have been plotted in Figs. 7 and 8, for the case of a rib with a dielectric constant of 13 and values of m equal to 0.4 and 0.8, respectively. For the sake of clarity, the scale of the abscissa has been changed at the ferrite-air interface. Within much of the ferrite the magnetic field is linearly polarized, with a small component of circular polarization. The energy distribution in the dielectric and ferrite regions differs widely for the two directions of propagation. This may explain, in part, the effectiveness of dielectric loading in phase shifters; the ferrite tends to displace the field outside the dielectric region for the negative wave. The maximum magnetic field intensity in the ferrite occurs in the region adjacent to the ferrite-dielectric interface. The field displacement effect is reduced for the lower value of m, but the fields are still strongly perturbed by the ferrite. The magnetic field intensity is shown in Fig. 9 for the case of ferrite slabs separated by an air gap. The structure dimensions are the same

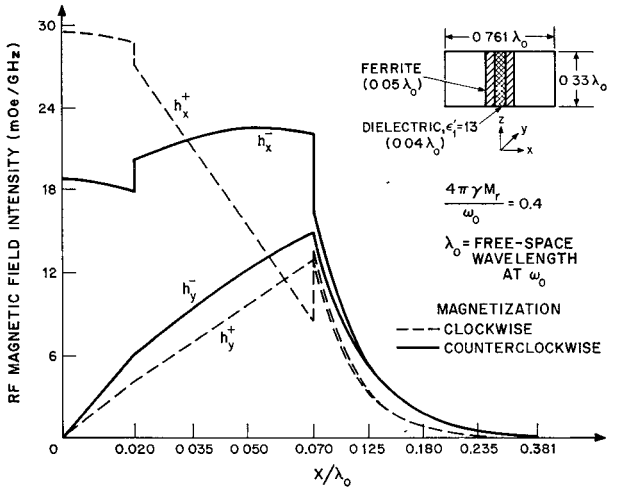

Fig. 7. Magnetic field intensity distribution for one watt of incident power.

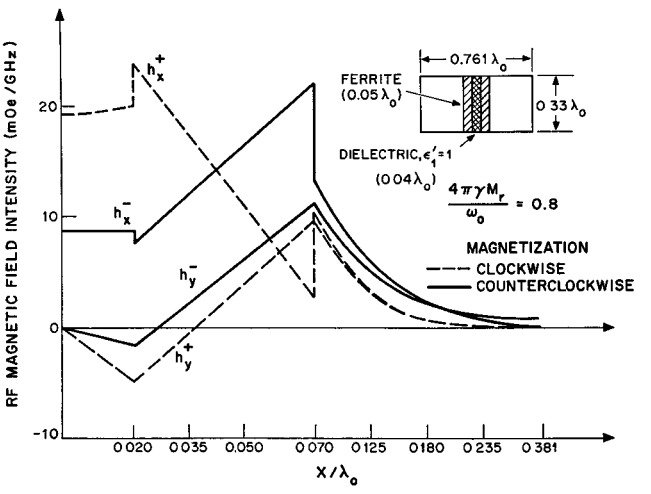

Fig. 9. Magnetic field intensity distribution for one watt of incident power.

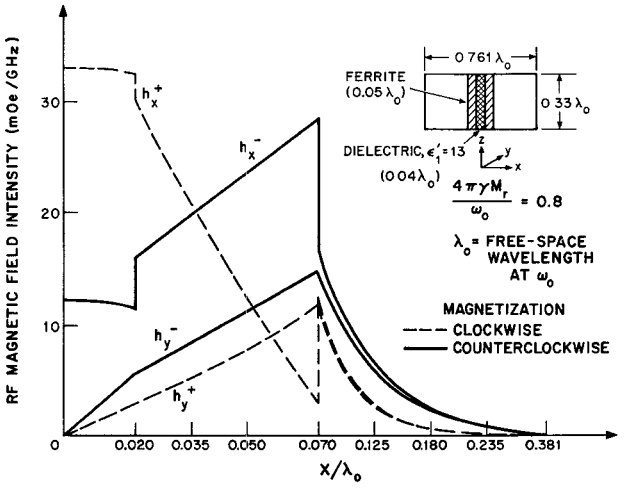

Fig. 8. Magnetic field intensity for one watt of incident power.

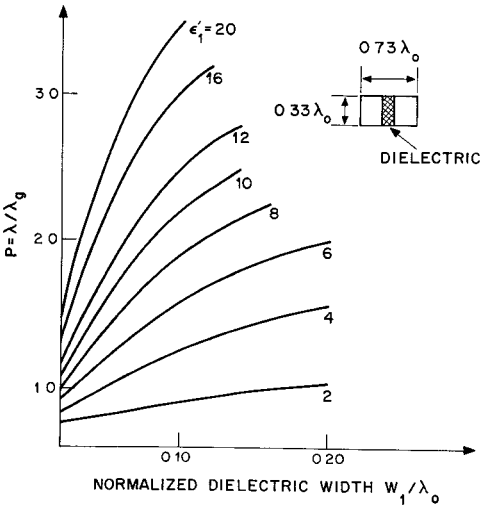

Fig. 10. Dielectrically loaded waveguide; normalized waveguide wavelength versus normalized dielectric width.

as in the previous figure. In general, the degree of field displacement is smaller than obtained with dielectric loading. This is consistent with the enhancement of differential phase shift expected with dielectric loading. However, the magnitude of the maximum magnetic field in the ferrite is not affected to any large extent by dielectric loading, as will be seen in Fig. 16. For wide waveguides the fields decay so rapidly away from the ferrite slabs that the side walls can be removed, with little effect on the phase shifter performance. The characteristic equation for the parallel plate waveguide configuration is readily obtained by setting $K_3 \cot \theta_3$ equal to α_3 in (8), where α_3 is the attenuation coefficient of the electric field in the x-direction within region 3.

Matching Networks for Phase Shifters

In a practical phase shifter, a matching network is required to match the phase shifter section to the connecting circuitry. One convenient type of matching structure is the n-section Tchebyscheff transformer [12], using dielectrically loaded waveguide sections. The basic design parameter, which is the wavelength λ_g of each section, may be readily obtained from the characteristic equation of the phase shifter by reducing the ferrite thickness to zero. Putting θ_2 equal to θ_4 in (5) leads to the following result,[2]

$$K_1 \cot \theta_1 = K_3 \cot \theta_3. \tag{13}$$

The solution to (13) may be obtained by an iterative process, similar to the method used for phase shifter characteristic equation. Some computed results are given in Fig. 10, which illustrates the parameter p as a function of dielectric width for a range of dielectric constants. The normalized waveguide width is 0.73 in this example.

[2] A similar calculation may be found in Marcuvitz [13]. I. Bardash and J. Klein in a private communication, and Taft [14] have reported similar calculations.

Experimental Results

A. Verification of Characteristic Equation

Experimental measurements have been made to test the theoretical computations on a number of phase shifter configurations over the X-band frequency range 8 to 11.5 GHz. The use of toroids in the remanent state for this purpose presented certain complications. For example, the connecting members which complete the magnetic path of the toroid are not accounted for in the model, and the flux in the connecting members is parallel to the broad walls of the waveguide. Thirdly, there are leakage flux effects. It was found that the corners of toroids contribute little to the observed differential phase shift. A corner correction factor F_c, equal to $(1-2W_4/W_5)$ in terms of the notation of Fig. 1, was applied to compensate for the discrepancy. A second important correction factor F_L was necessary to account for the flux leakage between the vertical ferrite members of the toroid(s), where

$$F_L \simeq 1 - \frac{\mu_0 H_c}{2B_r} \frac{W_5^2}{W_1 W_4}.$$

H_c is the coercive force and B_r is the remanent flux density of the ferrite. This formula represents the ratio of flux existing in the toroid walls with and without leakage effects. By assuming a uniform field equal to H_c to exist within the ferrite, the MMF drop across the slot was calculated, enabling an expression for the leakage flux to be obtained simply. The computed differential phase shift was multiplied by the product F_cF_L.

The ferrite and dielectric pieces of the experimental phase shifter were mounted in a section of precision rectangular waveguide. Broadband matching was accomplished by using dielectric tapers. Although adequate for our purposes, tapers are not to be recommended for practical phase shifters since, for adequate match, they are long and quite fragile. It was found that the residual air gaps between the dielectric rib and broad walls of the waveguide, and between the ferrite and waveguide, were the source of resonances which gave rise to regions of high VSWR. To eliminate this effect, the component pieces and the precision waveguide section were machined to a tolerance of 0.0002 inch.

It is to be expected that the performance of the double toroid phaser corresponds more closely to that of the ideal model than does the single toroid configuration. This is because the portions of the toroids, in the two-toroid configuration, not included in the ideal model are located in regions of low energy density. For this reason, differential phase shift measurements were performed on double toroid structures. Figure 11 shows the variation of differential phase shift as a function of frequency for a pair of toroids separated by an air gap. The data, obtained with a conventional microwave bridge, have been plotted for three different gap widths. For comparison the theoretical curves, adjusted to allow for the deviations from the ideal model, have been added. The agreement is good, particularly for the wide air gap case.

B. Low-Power Loss

A useful measure of the performance of a phase shifter is the loss per 2π section of differential phase shift $L_{2\pi}$. The low-power magnetic loss tangents have been measured by Temme [15], and his results are illustrated in Fig. 12. All of the measured loss tangents fall within the two straight lines shown and increase exponentially with the normalized saturation magnetization $4\pi\gamma M_s/\omega_0$, or m_s, where $4\pi M_s$ is the saturation magnetization. Note that the data have been plotted as a function of m_s, since it is this parameter which is related to the loss rather than the normalized remanence magnetization m.

It is emphasized that not all ferrite materials obey the empirical relationship shown in Fig. 12. In particular the temperature-compensated gadolinium-doped garnets would be represented by points lying to the left of the two straight lines in the figure. Also, for the materials shown the straight line approximation for values of μ'' in the range 0.0001 or less, which were not investigated, may not be valid. However, the curves can be used to give a useful qualitative description of phase shifter performance. An average loss characteristic, taken from Fig. 12, was incorporated into the computer program in order to estimate the behavior of $L_{2\pi}$ versus frequency. Solutions of (12) were obtained for a large number of phase shifter configurations. Some results of the analysis are given in Fig. 13, showing $L_{2\pi}$ versus F for several values of m_3. The wall resistance was taken to be 0.07 ohm per square and the dielectric loss tangent was 0.001 in each case. The latter figure is probably pessimistic. However, in practical phase shifters the losses due to cements and glues, etc., used in construction always cause the effective dielectric loss to be higher than expected. The dielectric and wall losses are predominant for small values of m_s and the device has to be extremely long to get appreciable phase shift, which accounts for the high uniform loss with frequency. For higher values of m_s, $L_{2\pi}$ decreases until optimum performance is obtained for m_s in the range 0.4 to 0.6. For values of m_s greater than 0.7, there is a rapid increase in $L_{2\pi}$ at the low end of the frequency band, due to the exponential nature of the low-power magnetic loss tangent versus m_s.

The insertion loss of two experimental phase shifters is plotted in Fig. 13. The measured values are corrected for corner and leakage losses. The loss as a function of frequency follows the predicted trends rather closely. The actual loss values need not agree with predicted values since the theoretical curves are for a hypothetical ferrite where loss tangent falls between the two lines in Fig. 12. The loss curves of the experimental ferrites appear to lie above this line.

The differential phase shift can be optimized by varying either the ferrite thickness (Fig. 4) or the dielectric width (Fig. 5). If ferrites whose loss tangent exceeds that of the dielectric are to be used, it is better to optimize with low-loss dielectric rather than ferrite in order to minimize the phase shifter loss.

Figure 14 shows the result of optimizing by varying the dielectric rib width, for a given value of m. It is seen that the minima are fairly broad. In this example, the loss is mainly

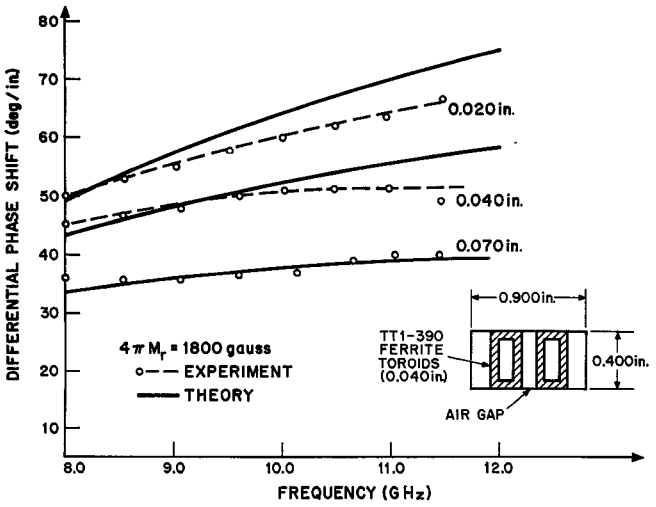

Fig. 11. Differential phase shift versus frequency for various air gaps.

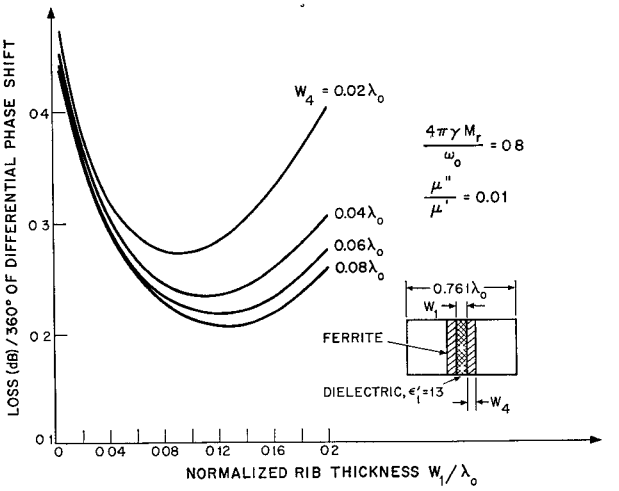

Fig. 14. Loss per 360° of differential phase shift versus dielectric thickness.

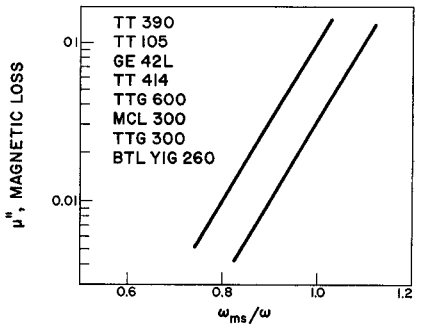

Fig. 12. Magnetic loss measurements.

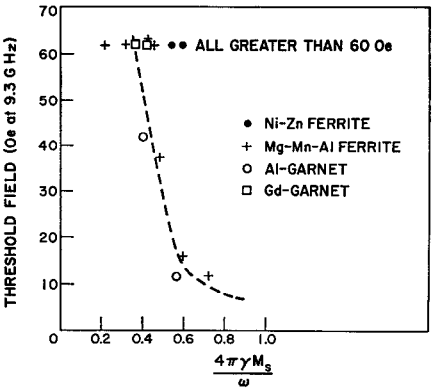

Fig 15.

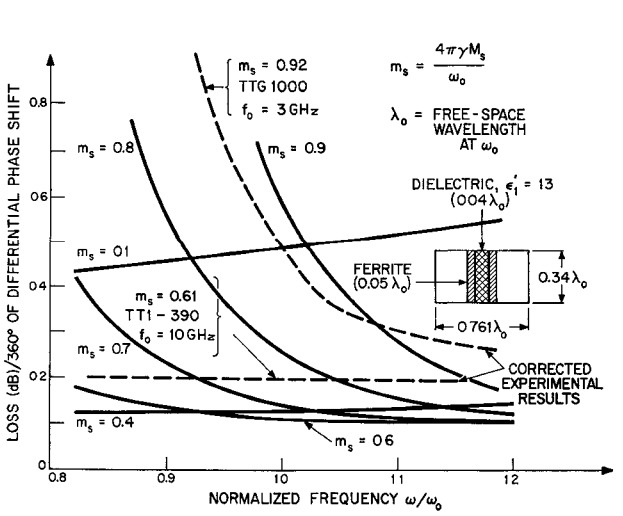

Fig. 13.

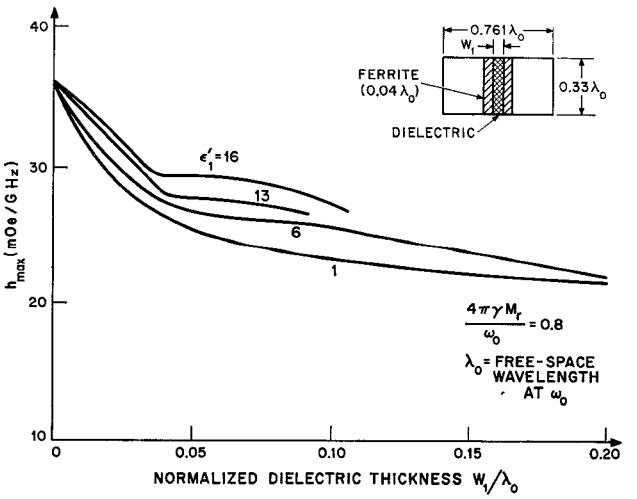

Fig. 16. Maximum magnetic field intensity in ferrite versus dielectric thickness for one watt of incident power.

magnetic in origin ($\mu''/\mu' = 0.01$, $\epsilon''/\epsilon' = 0.001$ for ferrite and dielectric) for values of W_1 less than $0.12\lambda_0$, and is predominantly due to dielectric and wall losses when W_1 is greater than $0.12\lambda_0$. Note that increasing the volume of ferrite actually causes $L_{2\pi}$ to decrease. This is because the additional ferrite results in a proportionately greater increase in differential phase shift (see Fig. 4).

C. High-Power Loss

At high-power levels, additional losses are incurred in the ferrite if the instability threshold for the excitation of spin wave instabilities is exceeded. Measurement of the instability threshold for various ferrites and garnets shows that it is a rapidly decreasing function of the parameter $(\gamma 4\pi M_s/\omega)$. Experimental data, illustrating this relationship, are plotted in Fig. 15. Similar trends have been observed by Killick [16] and Hair [17]. Note that reducing the magnetization for the purpose of raising h_{crit} also improves the low power performance, since $L_{2\pi}$ is correspondingly decreased. The experimental measurements of h_{crit} were performed on a double toroid phaser having a rib dielectric constant of 13. By referring to Figs. 7 and 8, the curves of magnetic field intensities in the waveguide, it can be seen that the maximum field intensity can occur at the center of the waveguide. Hence, in the case of a single toroid, the ferrite walls which are parallel to the broad faces of the waveguide contribute to an apparent lowering of the instability threshold. The value of m_s should probably be about 0.5 or less for a phaser operating in the 2- to 10-kW range in order to ensure that the instability threshold is not exceeded. Thus, both low- and high-power loss considerations limit the value of m_s.

The high power critical field can be raised considerably by other techniques; for example, by the introduction of strongly relaxing ions [18], such as Co^{2+}, Fe^{2+}, Ho^{2+}, and Dy^{2+}. However, this technique also causes the low power loss to be increased [18]. The ultimate choice of a suitable ferrite for a particular application involves a compromise between the low and high power requirements. Some improvement in peak power performance can be obtained by keeping the ferrite slabs well separated. In Fig. 16 the maximum RF field intensity, for one watt of incident power and normalized with respect to frequency, has been plotted as a function of dielectric rib thickness. It is seen that increasing the dielectric loading can increase the threshold power by about 2 to 1. Note that the variation of the rib dielectric constant has a smaller effect on the field intensity in the ferrite. Further increase in the peak power capacity can be achieved by increasing the waveguide height.

Conclusions

An idealized model, consisting of twin ferrite slabs in rectangular waveguide and separated by a dielectric rib, is a useful tool for predicting the performance of a class of nonreciprocal remanent phase shifters. The analysis presented in this paper enables the characteristic equation of the model to be derived in a form suitable for numerical solution by a computer. The predicted differential phase shift as a function of frequency has been calculated for various combinations of parameters. Substantial experimental verification of the theory has been obtained with a double toroid structure. Experimental data, illustrating the functional dependence of both low- and high-power loss on the magnetization, have been given. The results illustrate that optimum phase shifter performance is obtained if the ratio $\gamma 4\pi M_r/\omega$ is approximately equal to 0.5.

Acknowledgment

The authors wish to thank T. Barry and G. Maple for the reported measurements.

References

[1] D. H. Temme, "Progress and problems in high power phasers for array radar," *NEREM Rec.*, 1964.
[2] M. A. Treuhaft and L. M. Silber, "Use of microwave ferrite toroids to eliminate external magnets and reduce switching power," *Proc. IRE*, vol. 46, p. 1538, August 1958.
[3] E. Stern and H. Hair, "Development of helical time shifters," General Electric First Quart. Prog. Rept. to M.I.T. Lincoln Lab., under Subcontract 250, October 1961.
[4] H. P. J. Wijn, et al., "Conditions for square hysteresis loops in ferrite," *Phillips Tech. Rev.*, vol. 16, pp. 49–58, August 1954.
[5] B. Lax and K. T. Button, *Microwave Ferrites and Ferrimagnetics*. New York: McGraw-Hill, 1962, pp. 379–382.
[6] W. J. Ince and E. Stern, "Waveguide non-reciprocal remanence phase shifters," 1965 Proc. Int. Conf. on Microwave Behavior of Ferrimagnetics and Plasmas, *IEE (London)*.
[7] E. Schlömann, "Theoretical analysis of twin slab phase shifters in rectangular waveguide," *IEEE Trans. on Microwave Theory and Techniques*, vol. MTT-14, pp. 15–23, January 1966.
[8] E. Stern and A. Christopher, Microwave Chemicals. Lab., Final Rept. to M.I.T. Lincoln Lab., under Subcontract 291, May 1964.
[9] E. Stern and W. J. Ince, "Temperature stabilization of unsaturated microwave ferrite devices," 1965 11th Annual Conf. on Magnetism and Magnetic Materials, San Francisco, Calif.
[10] G. T. Rado, "Magnetic spectra of ferrites," *Rev. Mod. Phys.*, vol. 28, p. 81, January 1953.
[11] D. Polder and J. Smit, "Resonance phenomena in ferrites," *Rev. Mod. Phys.*, vol. 28, p. 89, January 1953.
[12] G. L. Matthaei et al., *Microwave Filters, Impedance-Matching Networks and Coupling Structures*. New York: McGraw-Hill, 1964, ch. 6.
[13] N. Marcuvitz, *Waveguide Handbook*. New York: McGraw-Hill, 1948.
[14] D. Taft, "Advanced ferrimagnetic materials applied to digital phase shifters," Sperry Microwave Electronics Co., Second Semi-Annual Rept. Program Code 4730.
[15] D. H. Temme, M.I.T. Lincoln Lab., private communication.
[16] E. Killick, "Problems of materials for high-power ferrite phase shifters for aerial scanning," Proc. Symp. on Electronically Scanned Array Techniques and Applications, Tech. Doc. Rept. RADC TDR 64-225, vol. 1, July 1964.
[17] H. Hair, "Development of helical phase shifters," General Electric, Final Rept. to M.I.T. Lincoln Lab., under Subcontract 250, December 1964.
[18] E. Schlömann and J. J. Green, "Ultimate performance limitations of high power ferrite circulators and phase shifters," *1965 Proc. INTERMAG*.